ACS OMEGA

http://pubs.acs.org/journal/acsodf

Article

High-Performance Mach–Zehnder Modulator Based on Thin-Film Lithium Niobate with Low Voltage-Length Product

Ying Li, Tian Lan,* Dengcai Yang, Jianfeng Bao, Meihua Xiang, Feng Yang, and Zhiyong Wang*

Cite This: *ACS Omega* 2023, 8, 9644–9651

Read Online

ACCESS | Metrics & More | Article Recommendations

ABSTRACT: Electro-optic modulators (EOMs) based on a thin-film lithium niobate (TFLN) photonic integration platform play a crucial role in loading electrical signals onto optical signals. In this paper, we proposed on-chip EOMs operating at two commercially available wavelengths of 850 and 1550 nm and successfully demonstrated rather low voltage-length products (V_π·Ls) of 0.78 V·cm and 1.29 V·cm, respectively. Additionally, the EOM working at 1550 nm exhibits the capability of 3-dB electro-optic (E-O) bandwidth beyond 40 GHz due to the limitation of our test conditions. This study is quite helpful for understanding EOM structures in a TFLN platform, as well as the fabrication of high-performance and multifunctional EOM devices.

1. INTRODUCTION

Electro-optic modulators (EOMs), used to convert electrical data into optical data, serve as a technological pillar of the modern telecommunication industry. Without these devices, telecommunication channels would be severely bandwidth-limited, particularly in data centers. To meet the ever-increasing bandwidth demands from the field of 5G,[1] satellite data links,[2] quantum information processing[3] and so on, EOMs with higher 3-dB electro-optic (E-O) bandwidth must be developed. Generally, materials, such as III–V compounds, conventional bulk lithium niobate (LN), and silicon, have already been widely used to fabricate commercial modulators. However, because of intrinsic nonlinearity, high cost, and the limitation of traditional waveguide fabrication techniques, neither III–V compounds nor bulk LN-based EOMs can meet the large-scale integration and low-cost requirements for the next-generation optical communication systems.[4−7] Thanks to the matured complementary metal-oxide-semiconductor (CMOS) fabrication process, silicon has become a major photonics platform but with the highest 3-dB E-O bandwidth only around 60 GHz due to the physical limitation of a free carrier dispersion effect.[8,9] Nowadays, with the success of manufacturing thin-film lithium niobate (TFLN)[10] and its breakthroughs in nanofabrication techniques,[11−19] the TFLN platform offers new possibilities for high-performance integrated nanophotonic systems. Therefore, EOMs based on the Pockels effect in TFLN have already outperformed their counterparts realized in traditional platforms.[20,21]

Owing to the high E-O coefficient of γ_{33} and the large refractive index contrast between the ridge waveguides core and cladding layer based on the FTLN platform, a 3-dB E-O bandwidth of more than 100 GHz and half-wave voltage (V_π) of 4.4 V have already been demonstrated in the device with a 5 mm E-O modulation region and reduced to 40 GHz and 1.4 V, respectively, when the modulation region increased to 20 mm.[22] The voltage-length product (V_π·L) is a commonly used parameter to describe the inverse relationship between the voltage required to modulate the output optical intensity of an EOM from a maximum to a minimum by applying a π phase shift and the physical length of the modulation region (L). Generally speaking, a lower V_π·L means a smaller device and potentially higher 3-dB E-O bandwidth to achieve a certain V_π. At present, the V_π·L of EOMs based on the TFLN platform, influenced by the distance between adjacent electrodes, the overlap of the normalized optical and electrical fields, and the effective refractive index of TFLN waveguides, is typically around 1.32–3.0 V.cm.[23−30] As a newly arisen EOM, the TFLN EOMs need to minimize the V_π·L to solve the problem of energy consumption to achieve energy-efficient communication. However, with the fast development of various photonic systems, the commercially available optical communication wavelength has been extended from the near-infrared band to the mid-infrared band; high-performance EOMs working at 1064 nm and 2 μm have been reported.[31,32] 850 nm, also as a frequently used optical communication wavelength, has been widely used in quantum communication and optical interconnection in data centers. Since the V_π is proportional to the working wavelength, a modulator at 850 nm has the notable advantage of a lower V_π. And an EOM operating at 850 nm wavelength with the 3-dB E-O bandwidth of 10 GHz has been reported in 2019, while the V_π·L is about 1.6 V·cm.[33]

In this paper, we demonstrated an on-chip TFLN EOM in the Mach–Zehnder-interferometer (MZI) configuration with coplanar waveguide (CPW) electrodes. Cosine-shaped Y-branch waveguides are applied to split the incident light into

Received: January 17, 2023
Accepted: February 14, 2023
Published: March 2, 2023

https://doi.org/10.1021/acsomega.3c00310
ACS Omega 2023, 8, 9644–9651

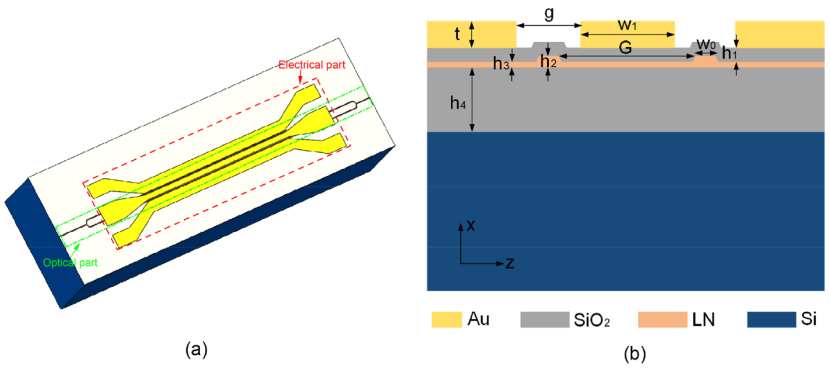

Figure 1. (a) The 3D schematic of the designed modulator, including the optical part (green arrow) and electrical part (red arrow). (b) Cross-section view of the TFLN waveguides in the modulation region of the designed modulator.

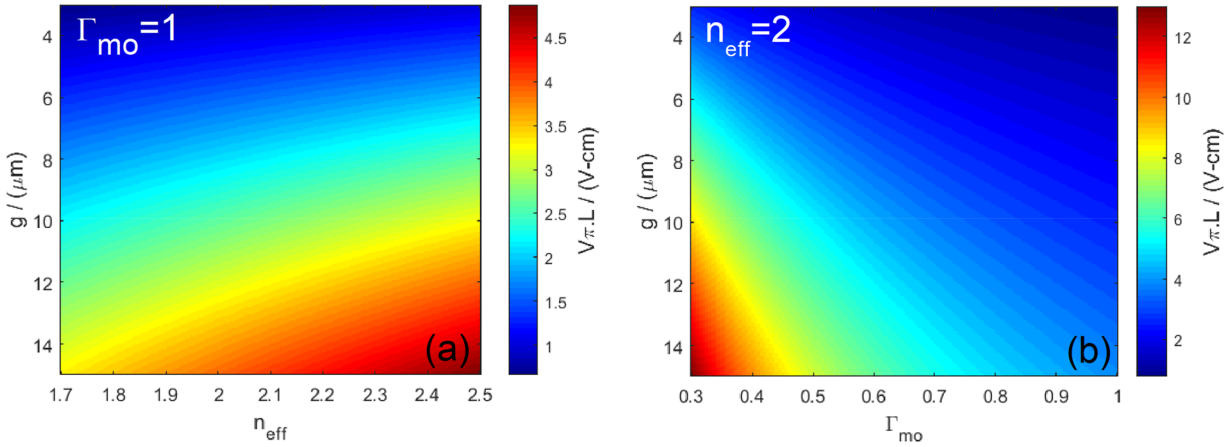

Figure 2. (a) $V_\pi \cdot L$ is evaluated as a function of n_{eff} and g at 1550 nm. (b) $V_\pi \cdot L$ is evaluated as a function of Γ_{mo} and g at 1550 nm.

both arms of the EOM and then combine again at the output facet. Our devices working at a wavelength of 1550 nm exhibit an on-chip insertion loss of −15 dB without a specially designed butt coupler, and the $V_\pi \cdot L$ is tested and calculated to be 1.29 V.cm, while the 3-dB E-O bandwidth is more than 40 GHz. Furthermore, we also reported an EOM operating at 850 nm with the lowest $V_\pi \cdot L$ of 0.78 V·cm, and the performance stability could be further enhanced by improving the butt coupling efficiency and the quality of the etching process.

2. MODULATOR DESIGN AND FABRICATION

The 3D schematic structure of the designed EOM based on the TFLN platform is shown in Figure 1a. A typical MZI configuration consists of two 3-mm-long modulation arms connected by cosine-shaped Y-branch couplers with an intersection angle of 2°,to achieve light splitting and combining. In order to reduce the fabrication difficulty of the deep etching, the TFLN is partially etched by 180 nm, and the top width of the waveguide is designed to 1.1 μm to ensure the guide optical mode in a waveguide working in only fundamental mode. And then, a pair of identical tapered waveguides, of which the top width is linearly changed from 1.1 to 2.5 μm over a length of 150 μm, is designed to connect the single-mode propagation waveguides and lensed fiber with a mode field diameter (MFD) of 2.5 μm. The electrical part of the EOM consists of two CPW gold electrodes with a push−pull configuration placed on both sides of the waveguides and a pair of ground−signal−ground (GSG) pads facilitating the high-speed microwave probing. The straight electrode tapers with 150 μm are designed to avoid extra RF loss caused by electrode bending. Figure 1b shows the cross-section view of the waveguides in the modulation arms. The TFLN, purchased from NanoLN,[34] includes a 400-nm-thick X-cut LN thin film bonded on a 4.7-μm-thick buried SiO_2 layer that is deposited on a 500-μm-thick Si substrate. Note that, to improve the spatial distribution of the electric field, realize velocity matching, and prevent excessive optical loss, a SiO_2 cladding layer is deposited on the top of the TFLN wafer. And, the push−pull configuration electrodes are placed on the SiO_2 cladding layer. In order to utilize the largest electro-optic coefficient γ_{33} component to achieve the highest modulation efficiency, light is set to propagate along the in-plane y axis, and the strongest component of the applied electric field of metal electrodes is designed along the z axis. The light is launched in the transverse electric mode, i.e., quasi-TE mode. And, the simulation results of this structure indicate one quasi-TE mode with an effective optical group index (n_g) of ∼2.21 and a loss of 0.00012 dB/cm by Lumerical Mode Solutions software.

2.1. Modulator Design. Based on electromagnetic theory,[35,36] the refractive index variation in the x-cut TFLN is given by eq 1:

$$\Delta n_{eff} = \frac{1}{2}\frac{n_e^4 r_{33}}{n_{eff}}\frac{V}{g}\Gamma_{mo} \quad (1)$$

where λ is the free-space wavelength, n_e is the material index of extraordinary rays, V is the modulation voltage, and Γ_{mo} is the normalized overlap between the optical and electric fields in the x−z plane, which can be expressed as eq 2:

https://doi.org/10.1021/acsomega.3c00310
ACS Omega 2023, 8, 9644−9651

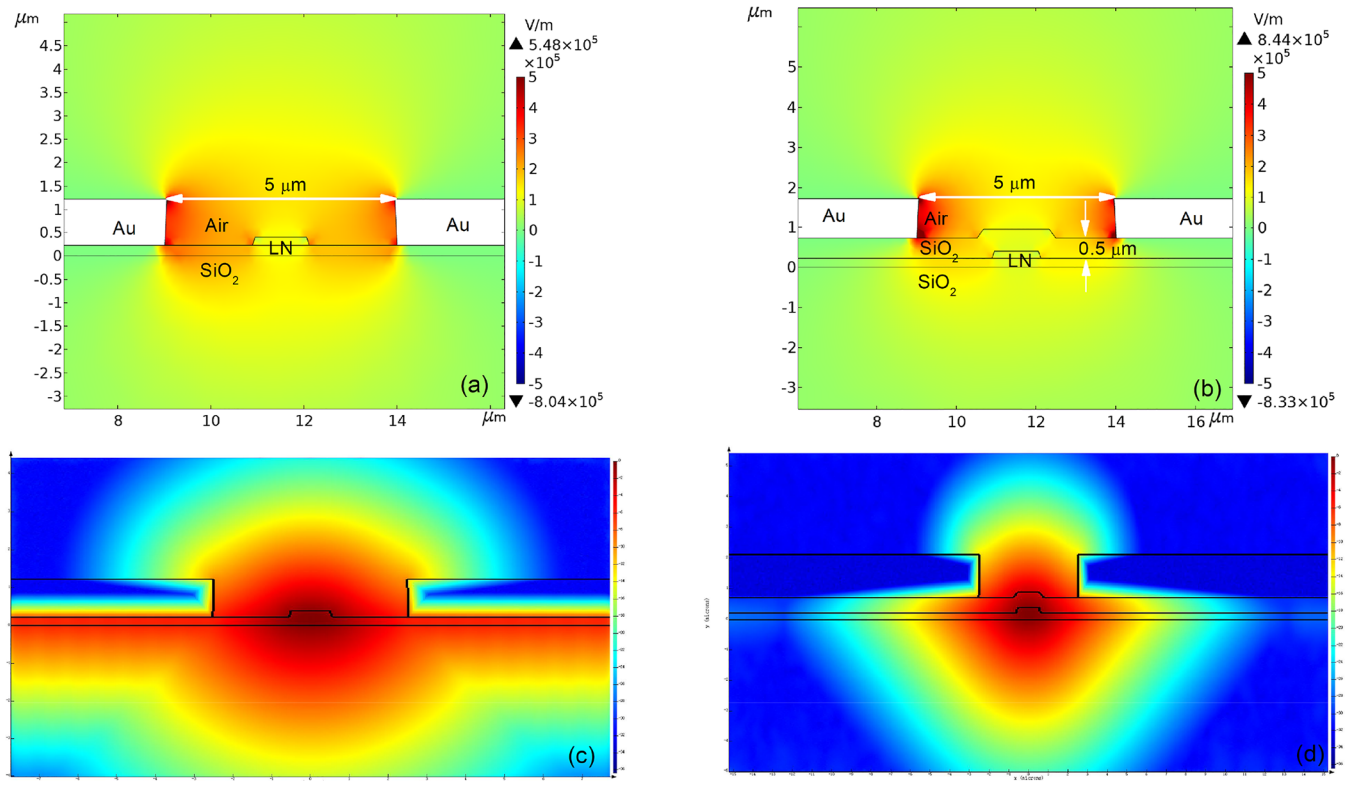

Figure 3. RF electric field of (a) the ridge waveguide structure commonly adopted in a TFLN modulator; (b) the ridge waveguide structure adopted in this work; the optical field with a logarithmic color scale of (c) the ridge waveguide structure commonly adopted in a TFLN modulator; (d) the ridge waveguide structure adopted in this work.

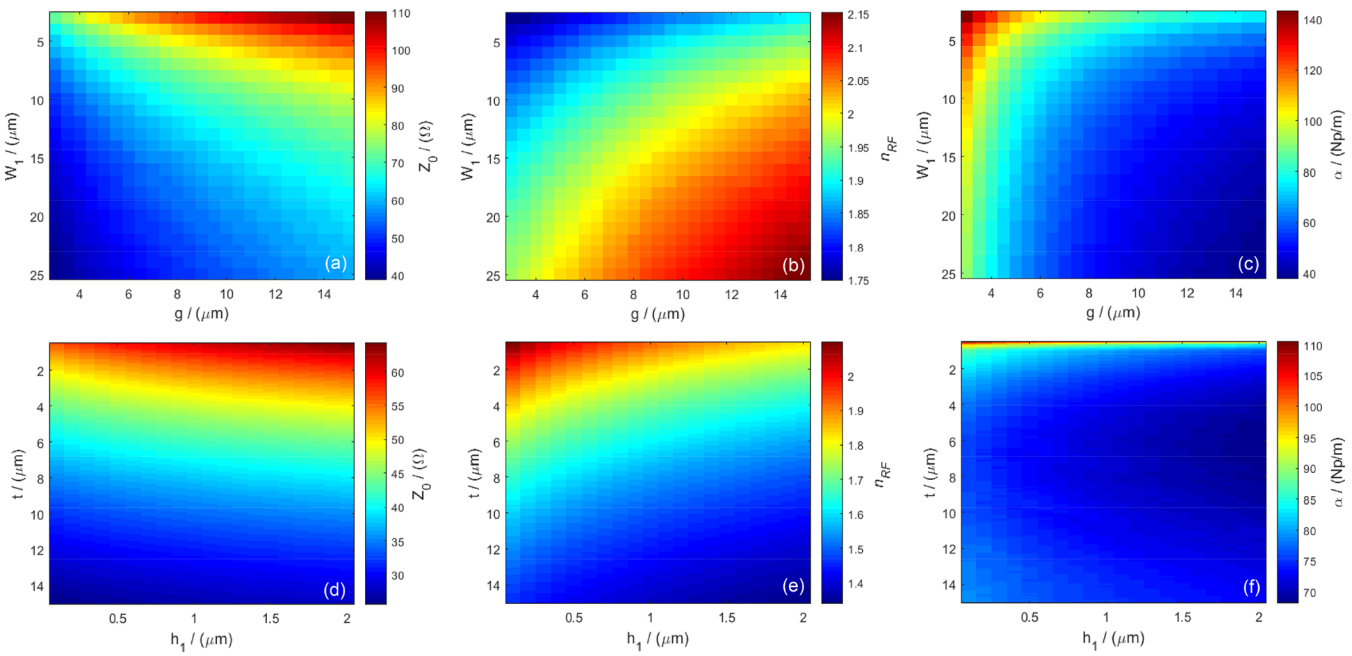

Figure 4. Calculated (a) Z_0, (b) n_{RF}, and (c) α of the modulation region of the modulator as a function of the width of the center electrode for the different designed gaps, when the t is 1 μm and h_4 is 2 μm. (d) Calculated (d) Z_0, (e) n_{RF}, and (f) α of the modulation region of the modulator as a function of the thickness of electrodes for the different designed thicknesses of the cladding layer, when the W_1 is 8 μm and g is 5 μm.

$$\Gamma_{mo} = \frac{g}{V}\frac{\iint_{ln} |E_o(xz)|^2 E_{RF}(x, z)\, dx\, dz}{\iint_{\infty} |E_o(x, z)|^2\, dx\, dz} \leq 1 \quad (2)$$

Here, E_o and E_{RF} are the optical and RF fields along the z direction, respectively. When the optical field is perturbed by an applied electric filed, the optical phase variation $\Delta\phi$ is calculated by eq 3:

$$\Delta\phi = \frac{n_e^4 r_{33} \pi V L}{n_{eff} \lambda g} \Gamma_{mo} \quad (3)$$

https://doi.org/10.1021/acsomega.3c00310
ACS Omega 2023, 8, 9644−9651

Table 1. Optimal Parameters of the Designed EOM at 1550 nm

parameters	W_1/ μm	t/ μm	g/ μm	h_1/ μm	h_2/ μm	h_3/ μm	H_4/ μm	W_0/ μm	G/ μm
value	18	1	5	0.5	0.4	0.22	4.7	1.1	25

If we set $\Delta\phi = \pi$, the $V_\pi \cdot L$ for the TFLN-based EOM in the push−pull conditions can be calculated using eq 4:

$$V_\pi L = \frac{1}{2} \times \frac{n_{\text{eff}} \lambda g}{n_e^4 \gamma_{33} \Gamma} \tag{4}$$

As shown in Figure 2, the theoretical limitation for $V_\pi \cdot L$ is between 0.66 and 13 V·cm when the three paramaters, i.e., n_{eff}, g, and Γ_{mo}, are set in a reasonable region, calculated using eq 4. However, n_{eff} plays a dominating role, especially when the Γ_{mo} is a constant. In principle, there are three key factors to guarantee high-performance operation of an EOM.[36] First of all, the EOM must be impedance matched, i.e., the characteristic impedance of the electrodes (Z_0) should be 50 Ω. Second, the difference between the microwave index (n_{RF}) in the transmission line and the group optical index in the waveguide should be as small as possible, indicating the electrical wave would propagate along with the CPW electrodes with the same velocity as the optical wave. At last, the microwave loss (α) must be as low as possible. However, it should be noticed that there are design trade-offs between bandwidth and working voltage. Figure 3b depicts the RF electric field of the structure adopted in our designed TFLN EOM; the peak RF electric field has increased by 57% compared with the structure in other works (as displayed in Figure 3a), which would greatly reduce the $V_\pi \cdot L$. Meanwhile, the corresponding optical fields with a logarithmic color scale are shown in Figure 3c and Figure 3d, respectively. It can be found that the optical field is strongly coupled to the leaky modes excited at the metal-LN interface without the SiO_2 cladding layer. The leaky mode distributed along the metal electrodes would lead to excessive optical loss for the EOM.

As we know, the bandwidth and voltage performances of the EOM are closely related to the structure of the electrode structure and the dielectric layer.[20,21,37,38] The electrode analysis operating at a frequency of 70 GHz using the variable-controlling approach is conducted via COMSOL Multiphysics was under the following initial conditions: the buried oxide layer thickness h_4 = 4.7 μm, the top SiO_2 cladding layer thickness h_1 = 1 μm, the electrode thickness t = 1 μm, the gap between top electrodes g = 5 μm, the signal electrode width W_1 = 10 μm, and the applied voltage V = 1 V. And the influence on the parameters of Z_0, n_{RF}, and α are illustrated in Figure 4. Compared with h_1 and t, W_1 and g show more significant impact on the propagation performance of CPW electrodes, since these parameters directly affect the value of distributed capacitance per unit length of the modulator region. The α and Z_0 both decrease with the increase of W, while the n_{RF} increases. In addition, because of the alleviation of electrical current congestion with the increase of g, α could be as low as ~0.96 dB/mm when g is beyond 5 μm. Considering that the electrode structure has complex effects on high-speed performance of the modulator, optimization simulations of the electrodes are carried out under the constraints of the minimum objective function by taking

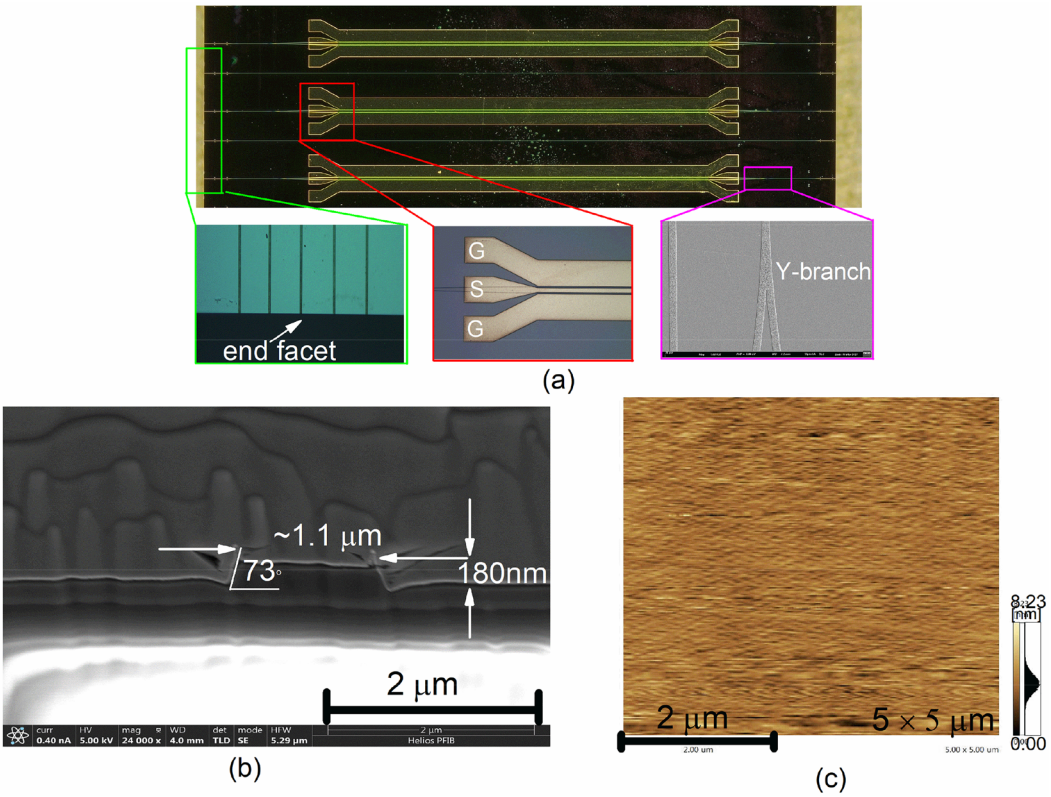

Figure 5. (a) Optical microscope images of the fabrication modulator. (b) SEM image of the cross-section of the fabrication waveguide. (c) AFM image of the dry etched surface of the sample.

https://doi.org/10.1021/acsomega.3c00310
ACS Omega 2023, 8, 9644−9651

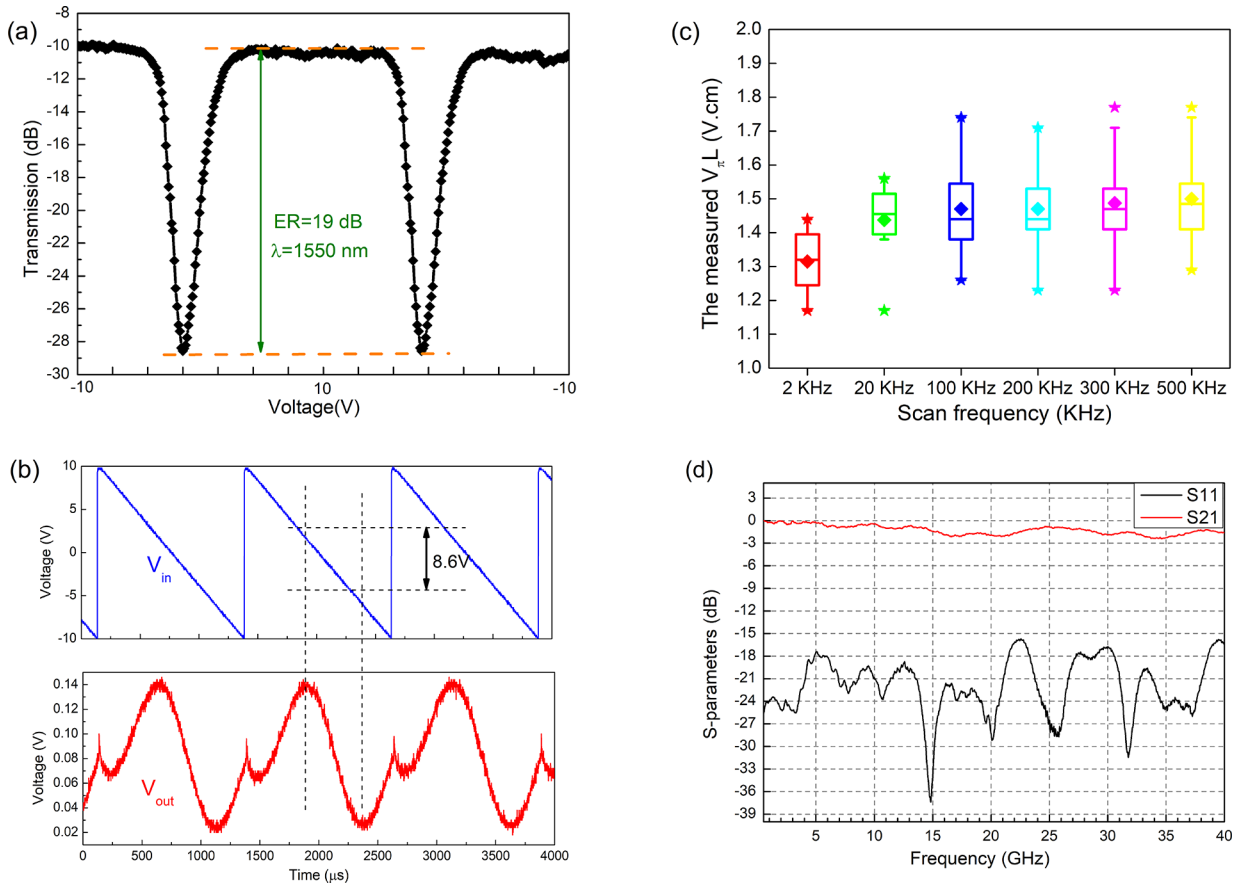

Figure 6. (a) The optical power versus applied DC voltage. (b) Voltage signals resulting from the designed EOM characterization. (c) $V_\pi \cdot L$ under different scanning speeds. (d) The measured E−O response of the modulator up to 40 GHz.

advantage of the optimization module in COMSOL Multiphysics; detailed results are listed in Table 1.

However, the three-dimensional structure of the designed EOM was simulated and analyzed in ANSYS HFSS, including GSG CPW electrodes and optical waveguides. The electrode structure consists of a probe region, a taper region, and an interaction region. The probe region includes three square rectangles with thae size of 100 × 100 μm, and the spacing between these probes is ∼50 μm. Then, Z_0 = 49 Ω and n_{RF} = 2.24 were obtained. Since in the case where the velocities of the optical wave and the microwave are matched, the 3-dB E-O bandwidth can be estimated by the 6.34-dB electrical loss.[20,36,37] Therefore, the theoretical E-O response of the designed EOM is evaluated by the loss of transmission line electrodes; according to the simulated curve of the microwave transmission S_{21} and reflection S_{11}, it is found that the EO response is much larger than 70 GHz, and the RF return loss is lower than −17 dB.

2.2. Modulator Fabrication. The fabrication approach for the designed EOM is as follows. First of all, a 400-nm-thick Cr layer was chosen as the hard mask and deposited on top of the cleaned TFLN wafer by using RF magnetron sputtering. Then, the waveguide pattern was defined by electro-beam lithography (EBL) and transferred to the Cr layer via a wetting-etched process. Subsequently, the wafer was etched in the mixture gases of SF_6 and Ar by inductively coupled plasma reactive ion etching (ICP-RIE). And the etching process was time-multiplexed to prevent the wafer from being damaged by overheating. After dry etching process, the Cr mask was wetting-etched using a mixture solution of $(NH_4)_2Ce(NO_3)_6$ and HNO_3, and the remaining photoresist was removed with acetone in a water bath. Then, a 500-nm-thick SiO_2 cladding layer was deposited on the TFLN using plasma-enhanced chemical vapor deposition (PECVD). As for the electrode definition, it is significantly different than electrode formation for the low-frequency EOM; electroplating was used instead of liftoff, to be much thicker. A thin seed layer of Ti/Au was first evaporated by electron beam evaporation (EBE) on the surface of the SiO_2 cladding layer. And then, the electrode patterns were fabricated through a secondary optical contact lithography process and an electroplating process. Finally, after the electrodes were as thick as 1 μm, the photoresist and uncovered seed layer were removed, and the end facets of the waveguides were diced to expose the waveguide end facets and carefully polished using a SiO_2 suspension in order to obtain a high coupling efficiency between the lens fibers.

The optical microscope images of our fabricated modulator with the enlarged image of electrodes and polished end fact of waveguides are shown in the Figure 5a; the size of the modulator is about 5.5 mm × 400 μm. Figure 5b shows the scanning electron microscope (SEM) image of the rib waveguides cross-section obtained by focused ion beam milling (FIB), it can be seen that the sidewall angle is about 73° and the etched depth of optical waveguides is 180 nm. And the root-mean-square (RMS) of the etched slab surface is measured to be 0.74 nm using an atomic force microscope (AFM) in the range of 5 × 5 μm^2 as displayed in Figure 5c. Note that the roughness of the etch slab surface significantly

https://doi.org/10.1021/acsomega.3c00310
ACS Omega 2023, 8, 9644−9651

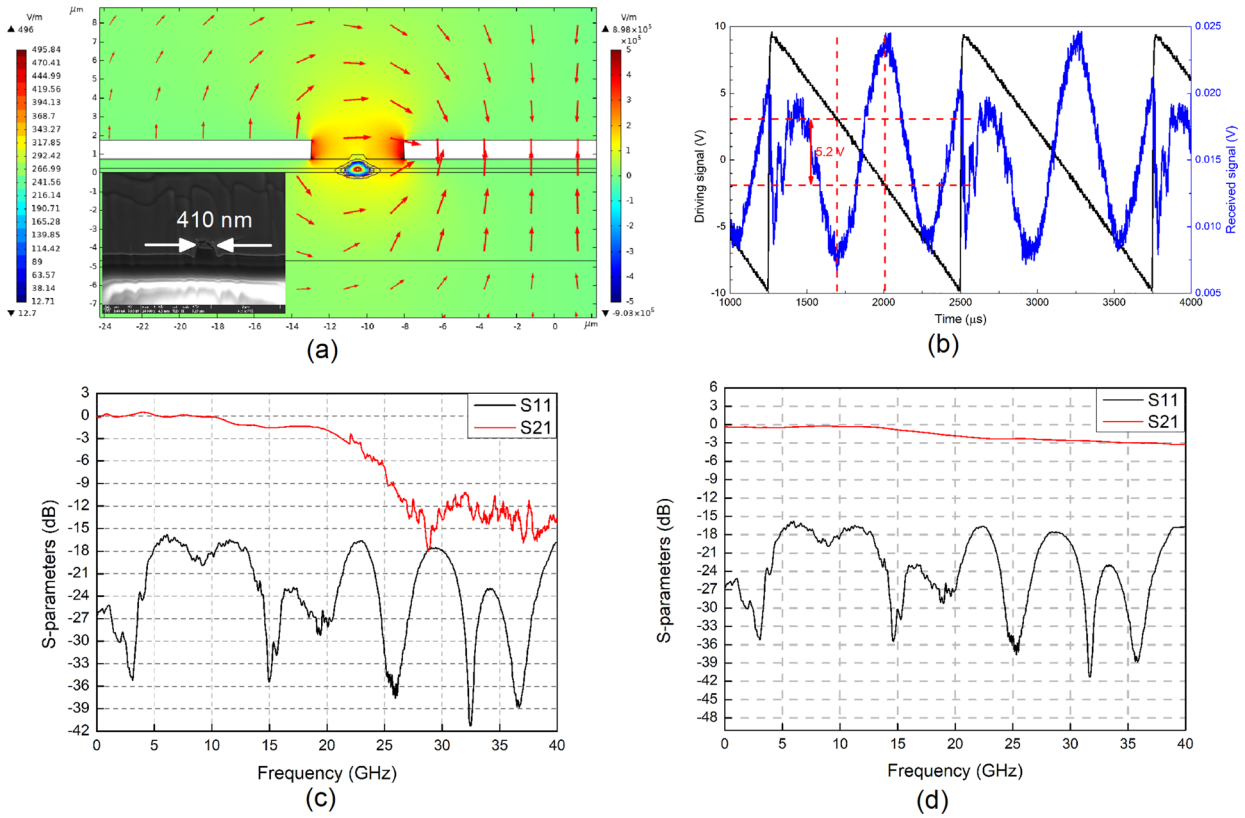

Figure 7. (a) The simulated overlap between the optical field and electric field via COMSOL Multiphysics at a frequency of 70 GHz at a wavelength of 850 nm (inset: the SEM image of the cross-section of the optical waveguide). (b) The measured non push−pull configuration voltage curve of the modulator under DC bias with 200 kHz. (c) The measured 3-dB E−O bandwidth of the fabricated modulator. (d) The measured 6.34-dB electrical loss of the fabricated modulator.

affects the flatness of the electrodes placed above, which could directly influence the microwave characterization of the devices.

3. RESULTS AND DISCUSSION

The experimental setup for the V_π measurement is as follows: for the optical signal, quasi-TE polarized light of 9 dBm from a tunable laser (KG-TLS, CONQUER) biased at 1550 nm wavelength is injected into the input waveguide of the modulator via butt-coupling by using a lensed fiber (CXFIBER). The modulated output light signal is measured using a highly sensitive InGaAs photodetector (KG-PR-200M-A, CONQUER) and then converted to a voltage signal (V_{out}) with a trans-impedance amplifier and finally observed on a digital oscilloscope (DSO: Tektronix). For the RF signal, a low frequency (∼2 kHz) sawtooth voltage signal (V_{in}) from a function generator (DG1022U, RIGOL) is divided into two branches: one is connected to the DSO directly, and the other is applied to the electrode of the EOM via the tungsten probe tips (Signatone SE-10T). (Ideally, the tungsten probes should be connected to the GSG pads of the EOM. However, due to the limitation of our test conditions, the tungsten probes were just connected to the GS pads; i.e., the EOM was tested in the nonpush−pull configuration.) It is worth noticing that for the V_π measurements at zero frequency, the other end of the CPW electrodes is left as an open circuit, and for nonzero frequency an extra load is necessary to prevent reflections and for impedance matching. Here, the plot of optical power versus applied DC voltage is shown in Figure 6a; it is found that the extinction ratio (ER) is 19 dB. And the voltage travel from the measurement at nonzero frequency is shown in Figure 6b, the measured non-push−pull value of V_π is 8.6 V. Therefore, the value of V_π for the designed modulator in push−pull configuration with a length of modulation arm of 3 mm is 4.3 V, of which the $V_\pi \cdot L$ is as low as 1.29 V·cm. Meanwhile, Figure 6c shows the box chart of the measured $V_\pi \cdot L$ under different scanning frequencies; it is found that at a low scanning frequency, the value of $V_\pi \cdot L$ is small, which probably is caused by the slow effect of LN.[39,40] What's more, as shown in Figure 6c, it can also be derived that the median of the $V_\pi \cdot L$ is no more than 1.5 V·cm. As for the measurement setup of high-frequency electro-optic characterization. It has been demonstrated that although the phase was adjusted via bias control, the insertion loss of the EOM is as high as 15 dB. Therefore, after the optical signal is modulated, the output light is amplified by an erbium doped fiber amplifier (EDFA) before being detected by a high-speed photodetector of 50 GHz (KG-PD-50G, CONQUER). Furthermore, the high-frequency RF signal from the vector network analyzer (VNA:ROHDE&SCHWARZ) is applied to the traveling-wave push−pull electrodes through a 40 GHz bandwidth input RF probe (Model 40A, GGB) and the RF signal is received by the RF probe connected with a 50 Ω load resistance to the electrodes. From Figure 6d, it can be found that the measured 3-dB E-O bandwidth of the fabricated modulator is larger than 40 GHz, and the microwave reflection is as low as −15 dB.

For the wavelength of 850 nm, the single-mode cutoff width is smaller than that of 1550 nm; therefore, the top width of the optical waveguide in our designed modulator is set to 410 nm,

https://doi.org/10.1021/acsomega.3c00310
ACS Omega 2023, 8, 9644−9651

and the etched depth is 180 nm. Additionally, the electrode structures are also simulated via optimization module of COMSOL Multiphysics. Based on the optimized results, a single electrode with a width of ∼16 μm is chosen for the visible modulator, and the overlap between optical field and electric field is evaluated as shown in Figure 7a. An optical power of −8 dBm was detected at the output port of the modulator when its input port was connected to a single-mode 850 nm semiconductor laser with an output power of 10 dBm. Since the same refractive index difference would cause a larger phase accumulation at a shorter wavelength, it is found that the calculated value of $V_\pi \cdot L$ in the push−pull configuration modulator with a gap between the electrodes of 5.5 μm in a modulation arm 3-mm-long is decrease to 0.78 V·cm. The E-O response of 850 nm EOM is shown in Figure 7c, the measured 3-dB E-O bandwidth is about 20 GHz. To be noted, it is limited by the bandwidth of our high-speed photodetector (KG-PD-20G, CONQUER) rather than the fabricated EOM itself. And to confirm this, the 6.34-dB electrical loss of this EOM is measured in Figure 7d and the 3-dB E-O bandwidth is far beyond 40 GHz. To the best of our knowledge, it is the first time that modulator working at 850 nm exhibited such a low half-wave voltage length product and high E-O response. However, since the insertion loss of the fabricated modulator has great influence on performance measurements, the stability of the device needs further improvements by designing an efficient butt coupler.

4. CONCLUSION

In this work, the on-chip EOMs based on the TFLN platform were designed and fabricated. The 3-dB E-O bandwidth is greater than 40 GHz according to theoretical calculation and experimental measurement. The modulator operating at 1550 nm shows a $V_\pi \cdot L$ no more than 1.5 V·cm. Furthermore, we also demonstrated a modulator working at 850 nm with the $V_\pi \cdot L$ = 0.78 V·cm. The corresponding 3-dB E-O bandwidth is beyond 40 GHz and beneficial for its applications in data center internal, optical interconnects and quantum communication.

AUTHOR INFORMATION

Corresponding Authors

Tian Lan − *Beijing Engineering Research Center of Laser Technology and Institute of Advanced Technology on Semiconductor Optics & Electronics, Institute of Laser Engineering, Beijing University of Technology, Beijing 100124, China; Key Laboratory of Trans-scale Laser Manufacturing Technology (Beijing University of Technology), Ministry of Education, Beijing 100124, China*; Email: lantian9094@bjut.edu.cn

Zhiyong Wang − *Beijing Engineering Research Center of Laser Technology and Institute of Advanced Technology on Semiconductor Optics & Electronics, Institute of Laser Engineering, Beijing University of Technology, Beijing 100124, China; Key Laboratory of Trans-scale Laser Manufacturing Technology (Beijing University of Technology), Ministry of Education, Beijing 100124, China*; Email: zywang@bjut.edu.cn

Authors

Ying Li − *Beijing Engineering Research Center of Laser Technology and Institute of Advanced Technology on Semiconductor Optics & Electronics, Institute of Laser Engineering, Beijing University of Technology, Beijing 100124, China; Key Laboratory of Trans-scale Laser Manufacturing Technology (Beijing University of Technology), Ministry of Education, Beijing 100124, China*; orcid.org/0000-0003-1696-7569

Dengcai Yang − *Beijing Engineering Research Center of Laser Technology and Institute of Advanced Technology on Semiconductor Optics & Electronics, Institute of Laser Engineering, Beijing University of Technology, Beijing 100124, China; Key Laboratory of Trans-scale Laser Manufacturing Technology (Beijing University of Technology), Ministry of Education, Beijing 100124, China*

Jianfeng Bao − *Beijing Engineering Research Center of Laser Technology and Institute of Advanced Technology on Semiconductor Optics & Electronics, Institute of Laser Engineering, Beijing University of Technology, Beijing 100124, China; Key Laboratory of Trans-scale Laser Manufacturing Technology (Beijing University of Technology), Ministry of Education, Beijing 100124, China*

Meihua Xiang − *Beijing Engineering Research Center of Laser Technology and Institute of Advanced Technology on Semiconductor Optics & Electronics, Institute of Laser Engineering, Beijing University of Technology, Beijing 100124, China; Key Laboratory of Trans-scale Laser Manufacturing Technology (Beijing University of Technology), Ministry of Education, Beijing 100124, China*

Feng Yang − *Beijing Engineering Research Center of Laser Technology and Institute of Advanced Technology on Semiconductor Optics & Electronics, Institute of Laser Engineering, Beijing University of Technology, Beijing 100124, China; Key Laboratory of Trans-scale Laser Manufacturing Technology (Beijing University of Technology), Ministry of Education, Beijing 100124, China*

Complete contact information is available at: https://pubs.acs.org/10.1021/acsomega.3c00310

Author Contributions

Ying Li, Tian Lan, Dengcai Yang, and Zhiyong Wang initiated the project and conceived the experiments. Ying Li designed and fabricated the devices. Ying Li and Jianfeng Bao conducted experimental measurements. Meihua Xiang and Feng Yang performed supporting experiments. Ying Li conducted simulations and data analysis. Dengcai Yang and Zhiyong Wang provided suggestions throughout the project. Tian Lan and Zhiyong Wang supervised the project. All authors discussed the results and commented on the manuscript.

Funding

This work was supported by the Central Military Commission Equipment Advance research project field fund under grant no. 80914020105.

Notes

The authors declare no competing financial interest.

ACKNOWLEDGMENTS

The authors would like to acknowledge PANWOO Integrated Optoelectronic Inc. for supporting part of the experiments.

REFERENCES

(1) Lu, G. W.; Hong, J.; Qiu, F.; Spring, A. M.; Yokoyama, S. Author Correction: High-temperature-resistant silicon-polymer hybrid modulator operating at up to 200 Gbit/s for energy-efficient datacentres and harsh-environment applications. *Nat. Commun.* **2020**, *11* (1), 1−9.

(2) Cheng, L.; Aditya, S.; Nirmalathas, A. An exact analytical model for dispersive transmission in microwave fiber-optic links using Mach-Zehnder external modulator. *IEEE Photonics Technology Letters* **2005**, *17* (7), 1525−1527.
(3) Marpaung, D.; Yao, J.; Capmany, J. Integrated microwave photonics. *Nat. Photonics* **2019**, *13* (2), 80−90.
(4) Ogiso, Y.; Hashizume, Y.; Tanobe, H.; Nunoya, N.; Ida, M.; Miyamoto, Y.; Ishikawa, M.; Ozaki, J.; Ueda, Y.; Wakita, H.; Nagatani, M.; Yamazaki, H.; Nakamura, M.; Kobayashi, T.; Kanazawa, S. 80-GHz Bandwidth and 1.5-V Vπ InP-based IQ Modulator. *Journal of Lightwave Technology* **2020**, *38* (2), 249−255.
(5) Dogru, S.; Dagli, N. 0.77-V drive voltage electro-optic modulator with bandwidth exceeding 67 GHz. *Optics letters* **2014**, *39* (20), 6074−6077.
(6) Bhasker, P.; Norman, J.; Bowers, J. E.; Dagli, N. Low Voltage, High Optical Power Handling Capable, Bulk Compound Semiconductor Electro-Optic Modulators at 1550 nm. *Journal of Lightwave Technology* **2020**, *38* (8), 2308−2314.
(7) Wooten, E.L.; Kissa, K.M.; Yi-Yan, A.; Murphy, E.J.; Lafaw, D.A.; Hallemeier, P.F.; Maack, D.; Attanasio, D.V.; Fritz, D.J.; McBrien, G.J.; Bossi, D.E. A review of lithium niobate modulators for fiber-optic communications systems. *IEEE J. Sel. Top. Quantum Electron.* **2000**, *6* (1), 69−82.
(8) Gardes, F. Y.; Reed, G. T.; Emerson, N. G.; Png, C. E. A sub-micron depletion-type photonic modulator in Silicon On Insulator. *Opt. Express* **2005**, *13* (22), 8845−8854.
(9) Li, Z. Y.; Xu, D. X.; Mckinnon, W. R.; Janz, S.; Schmid, J. H.; Cheben, P.; Yu, J. Z. Silicon waveguide modulator based on carrier depletion in periodically interleaved PN junctions. *Opt. Express* **2009**, *17* (18), 15947−15958.
(10) Rabiei, P.; Gunter, P. Optical and electro-optical properties of submicrometer lithium niobate slab waveguides prepared by crystal ion slicing and wafer bonding. *Appl. Phys. Lett.* **2004**, *85* (20), 4603−4605.
(11) Cai, L.; Kang, Y.; Hu, H. Electric-optical property of the proton exchanged phase modulator in single-crystal lithium niobate thin film. *Opt. Express* **2016**, *24* (5), 4640−4647.
(12) Wang, Y.; Chen, Z.; Cai, L.; Jiang, Y.; Zhu, H.; Hu, H. Amorphous silicon-lithium niobate thin film strip-loaded waveguides. *Optical Materials Express* **2017**, *7* (11), 4018−4028.
(13) Li, Y.; Lan, T.; Yang, D.; Wang, Z. Fabrication of ridge optical waveguide in thin film lithium niobate by proton exchange and wet etching. *Opt. Mater.* **2021**, *120* (17), 111433.
(14) Wang, C.; Zhang, M.; Stern, B.; Lipson, M.; Loncar, M. Nanophotonic Lithium Niobate Electro-optic Modulators. *Opt. Express* **2018**, *26* (2), 1547−1555.
(15) Krasnokutska, I.; Tambasco, J. J.; Li, X.; Peruzzo, A. Ultra-low loss photonic circuits in lithium niobate on insulator. *Opt. Express* **2018**, *26* (2), 897−904.
(16) Hu, H.; Ricken, R.; Sohler, W. Lithium niobate photonic wires. *Opt. Express* **2009**, *17* (26), 24261−24268.
(17) Chun-Ming, C.; Chih-Sheng, Y.; Fan-Chun, H.; Chun-Ting, L.; Tsung-Tao, H.; et al. A parametric study of ICP-RIE etching on a lithium niobate substrate. *10th IEEE International Conference on Nano/Micro Engineered and Molecular Systems*, Xi'an, China, 2015; IEEE, 2015; pp 485−486, DOI: 10.1109/NEMS.2015.7147473.
(18) Li, X. P.; Chen, K. X.; Hu, Z. F. Low-loss bent channel waveguides in lithium niobate thin film by proton exchange and dry etching. *Optical Materials Express* **2018**, *8* (5), 1322−1327.
(19) Qu, M.; Shen, Y.; Wu, L.; Fu, X.; Cheng, X.; Wang, Y. Homogenous and ultra-shallow lithium niobate etching by focused ion beam. *Precision Engineering* **2020**, *62*, 10−15.
(20) Zhang, M.; Wang, C.; Kharel, P.; Zhu, D.; Lončar, M. Integrated lithium niobate electro-optic modulators: when performance meets scalability. *Optica* **2021**, *8* (5), 652−667.
(21) Sinatkas, G.; Christopoulos, T.; Tsilipakos, O.; Kriezis, E. E. Electro-optic modulation in integrated photonics. *J. Appl. Phys.* **2021**, *130* (1), 010901.
(22) Wang, C.; Zhang, M.; Chen, X.; Bertrand, M.; Shams-Ansari, A.; Chandrasekhar, S.; Winzer, P.; Loncar, M. Integrated lithium niobate electro-optic modulators operating at CMOS-compatible voltages. *Nature* **2018**, *562* (7725), 101−112.
(23) Jin, S.; Xu, L.; Zhang, H.; Li, Y. LiNbO3 Thin-Film Modulators Using Silicon Nitride Surface Ridge Waveguides. *IEEE Photonics Technology Letters* **2016**, *28* (7), 736−739.
(24) He, M. B.; Xu, M. Y.; Ren, Y. X.; Jian, J.; Ruan, Z. L.; Xu, Y. S.; Gao, S. Q.; Sun, S. H.; Wen, X. Q.; Zhou, L. D.; et al. High-performance hybrid silicon and lithium niobate Mach-Zehnder modulators for 100 Gbit/s and beyond. *Nat. Photonics* **2019**, *13* (5), 359−364.
(25) Ahmed, A. N. R.; Nelan, S.; Shi, S.; Yao, P.; Mercante, A.; Prather, D. W. Sub-volt electro-optical modulator on thin-film lithium niobate and silicon nitride hybrid platform. *Optics letters* **2020**, *45* (5), 1112−1115.
(26) Liu, Y.; Li, H.; Liu, J.; Tan, S.; Lu, Q.; Guo, W. Low Vπ thin-film lithium niobate modulator fabricated with photoliography. *Opt. Express* **2021**, *29* (5), 6320−6329.
(27) Liu, X.; Xiong, B.; Sun, C.; Wang, J.; Hao, Z.; Wang, L.; Han, Y.; Li, H.; Yu, J.; Luo, Y. Wideband thin-film lithium niobate modulator with low half-wave-voltage length product. *Chinese Optics Letters* **2021**, *19* (6), 060016.
(28) Jin, M.; Chen, J.; Sua, Y.; Kumar, P.; Huang, Y. Efficient electro-optical modulation on thin-film lithium niobate. *Optics letters* **2021**, *46* (8), 1884−1887.
(29) Jin, M.; Chen, J.; Sua, Y.; Kumar, P.; Huang, Y. Efficient electro-optical modulation on thin-film lithium niobate: erratum. *Optics letters* **2021**, *46* (18), 4601−4601.
(30) Xu, M.; Zhu, Y.; Pittalà, F.; Tang, J.; He, M.; Ng, W. C.; Wang, J.; Ruan, Z.; Tang, X.; Kuschnerov, M.; et al. Dual-polarization thin-film lithium niobate in-phase quadrature modulators for terabit-per-second transmission. *Optica* **2022**, *9* (1), 61−62.
(31) Jagatpal, N.; Mercante, A. J.; Ahmed, A. N. R.; Prather, D. W. Thin Film Lithium Niobate Electro-Optic Modulator for 1064 nm Wavelength. *IEEE Photonics Technology Letters* **2021**, *33* (5), 271−274.
(32) Pan, B.; Hu, J.; Huang, Y.; Song, L.; Wang, J.; Chen, P.; Yu, Z.; Liu, L.; Dai, D. Demonstration of high-speed thin-film lithium-niobate-on-insulator optical modulators at the 2-microm wavelength. *Opt. Express* **2021**, *29* (12), 17710−17717.
(33) Desiatov, B.; Shams-Ansari, A.; Zhang, M.; Wang, C.; Lončar, M. Ultra-low-loss integrated visible photonics using thin-film lithium niobate. *Optica* **2019**, *6* (3), 380−384.
(34) Jinan Jingzheng Electronics Co., Ltd. (NANOLN, Inc.). https://www.nanoln.com/.
(35) Toney, J. E. *Lithium Niobate Photonics*; Artech House, 2015.
(36) Weigel, P. O. *High-Speed Hybrid Silicon-Lithium Niobate Electro-Optic Modulators & Related Technologies*; University of California, San Diego, 2018.
(37) Yang, F.; Fang, X.; Chen, X.; Zhu, L.; Zhang, F.; Chen, Z.; Li, Y. Monolithic thin film lithium niobate electro-optic modulator with over 110 GHz bandwidth. *Chinese Optics Letters* **2022**, *20* (2), 022502.
(38) Zhu, D.; Shao, L.; Yu, M.; Cheng, R.; Desiatov, B.; Xin, C. J.; Hu, Y.; Holzgrafe, J.; Ghosh, S.; Shams-Ansari, A.; Puma, E.; Sinclair, N.; Reimer, C.; Zhang, M.; Loncar, M. Integrated photonics on thin-film lithium niobate. *Advances in Optics and Photonics* **2021**, *13* (2), 242−352.
(39) Salvestrini, J. P.; Guilbert, L.; Fontana, M.; Abarkan, M.; Gille, S. Analysis and Control of the DC Drift in $LiNbO_3$-Based Mach−Zehnder Modulators. *Journal of Lightwave Technology* **2011**, *29* (10), 1522−1534.
(40) Liu, X.; Xiong, B.; Sun, C.; Wang, J.; Hao, Z.; Wang, L.; Han, Y.; Li, H.; Yu, J.; Luo, Y. Wideband thin-film lithium niobate modulator with low half-wave-voltage length product. *Chinese Optics Letters* **2021**, *19* (6), 060016.

https://doi.org/10.1021/acsomega.3c00310
ACS Omega 2023, 8, 9644−9651